Momentum-selective pair creation of spin excitations in dipolar bilayers

Thomas Bilitewski,[1] G. A. Domínguez-Castro,[2] David Wellnitz,[3,4] Ana Maria Rey,[3,4] and Luis Santos[2]

[1]*Department of Physics, Oklahoma State University, Stillwater, Oklahoma 74078, USA*
[2]*Institut für Theoretische Physik, Leibniz Universität Hannover, Appelstr. 2, D-30167 Hanover, Germany*
[3]*JILA, National Institute of Standards and Technology and Department of Physics, University of Colorado, Boulder, CO, 80309, USA*
[4]*Center for Theory of Quantum Matter, University of Colorado, Boulder, CO, 80309, USA*

(Dated: February 20, 2023)

We study the temporal growth and spatial propagation of quantum correlations in a two-dimensional bilayer realising a spin-1/2 quantum XXZ model with couplings mediated by long-range and anisotropic dipolar interactions. Starting with an initial state consisting of spins with opposite magnetization in each of the layers, we predict the emergence of a momentum-dependent dynamic instability in the spin structure factor that results, at short times, in the creation of pairs of excitations at exponentially fast rates. The created pairs present a characteristic momentum distribution that can be tuned by controlling the dipolar orientation, the layer separation or the dipolar couplings. The predicted behavior remains observable at very low filling fractions, making it accessible in state-of-the-art experiments with Rydberg atoms, magnetic atoms, and polar molecule arrays.

Anisotropic dipolar interactions controllable via electromagnetic fields offer unique opportunities for the implementation of iconic models of quantum magnetism relevant for fundamental science and for the development of novel quantum technologies. In recent years, great progress has been made on the implementation of dipole-induced spin exchange interactions in fully controllable quantum systems of polar molecules [1–3], magnetic atoms [4] and Rydberg atoms [5, 6]. However, most of the investigations so far have been targeted to the single excitation regime [7] or to the case of multiple excitations characterized via collective observables [8–17]. Nevertheless, recent experimental developments on quantum gas microscopes [18, 19] and optical tweezers [20–24] that allow for the spatial-resolved control of correlations at the single particle level are opening a window to explore rich and intriguing quantum phenomena enabled by dipolar spin models.

In this work, we study the temporal and spatial growth of correlations during the many-body dynamics of an array of spin-1/2 frozen dipoles confined in two separated two-dimensional layers (see Fig. 1(a)). This system, implementable for example using optical lattices or tweezer arrays, realises a quantum XXZ spin model with dipolar couplings. By preparing the two layers in opposite spin states, as in recent experiments on polar molecules [15], one creates a dynamically unstable state from which correlated pairs of spin excitations develop and grow at an exponential rate, at least at short times. These correlated pairs manifest in the spin structure factor, which develops intriguing momentum patterns controllable by both the separation of the layers, and the magnitude and orientation of the dipole moments.

The build up of spin correlations can be explained using a Bogoliubov analysis, which uncovers a dynamical instability in specific tunable momentum modes. We validate the Bogoliubov predictions of the pair creation patterns by numerical simulations of the full spin dynamics, and show that pattern formation remains robust even for very low lattice fillings, making it observable in state of the art experiments, without requiring unit-filling.

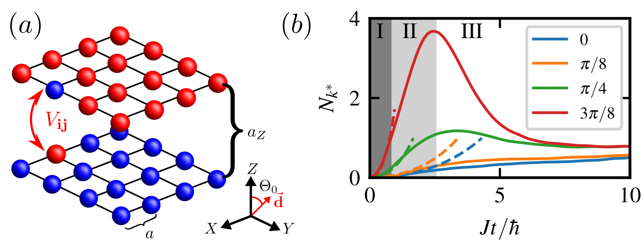

FIG. 1. System. (a) Bilayer of dipoles confined in 2D planes with dipole moments aligned at an angle Θ_0 to the out-of-plane direction. When the layers are prepared in an initial state with opposite magnetization, dipolar inter-layer interactions create pairs of excitations in the layers in specific quasi-momentum modes. (b) Occupation of the most unstable mode N_{k^*} as a function of time t for different dipole orientations Θ_0 (legend) at fixed $a_Z/a = 2$. Shown are spin dynamics from DTWA (solid lines), and the prediction from Bogoliubov theory (dashed lines). Shaded regions indicate the regimes of dynamics (for $\Theta_0 = 3\pi/8$), where we find exponential growth as predicted by Bogoliubov (I), saturation and slow-down of growth (II), and eventual decay and thermalisation (III). Results for a 33×33 bilayer at unit filling.

The predicted instabilities and exponential proliferation of correlated pairs of excitations between spatially separated layers, which emulate the phenomenon of pair creation from vacuum fluctuations, open unique opportunities for quantum simulation, and for fundamental tests of quantum mechanics including EPR steering [25–28]. Pair creation itself is an ubiquitous phenomenon in physics, relevant in a broad range of contexts including parametric amplification and two-mode squeezing in quantum optics [29], the Schwinger effect in high energy physics [30–32], the emission of Unruh thermal radiation in curved space time [33, 34], and in holography given that the thermofield double state generated during pair production is dual to a traversable wormhole [35, 36] in quantum gravity, and a resource for quantum teleportation [37–39].

Previous studies of pair creation processes in spinor condensates induced by contact interactions [40–43] were dominated by single (resonant) momentum modes (or trap states in confined condensates [44]) determined by the quadratic Zeeman shift, while proposals of pair production in cavities induced by collective interactions [45] require a set of laser tones to generate non-trivial patterns, and are sensitive to cavity loss [46]. In contrast, the pair creation observed in this work allows for the generation of highly tunable, and intriguing distributions of excitations naturally emerging from anisotropic dipolar couplings [1–4, 8–11, 13, 47, 48].

Model: We consider an array of frozen dipoles with two relevant internal levels (e.g. two rotational states in the case of polar molecules) confined in two parallel two-dimensional layers generated via optical lattices or optical tweezers, separated by a tunable distance a_Z. We denote the upper layer as A and the lower one as B. As shown in Fig. 1(a), both layers have square geometry with a nearest-neighbour spacing a.

Electric and magnetic dipole-dipole interactions can lead to both exchange of internal-state excitations, as well as Ising interactions [7–13, 47, 49], which can be tuned via external electromagnetic fields. For the case of frozen particles, the dynamics is governed by the celebrated (long-range) spin-1/2 XXZ model:

$$\hat{H}_{XXZ} = \frac{1}{2}\sum_{\sigma=A,B}\sum_{\mathbf{i}\neq\mathbf{j}} V^{\sigma\sigma}_{\mathbf{ij}}(\hat{s}^+_{\mathbf{i}\sigma}\hat{s}^-_{\mathbf{j}\sigma} + \hat{s}^-_{\mathbf{i}\sigma}\hat{s}^+_{\mathbf{j}\sigma} + 2\eta\hat{s}^z_{\mathbf{i}\sigma}\hat{s}^z_{\mathbf{j}\sigma}) + \sum_{\mathbf{i},\mathbf{j}} V^{AB}_{\mathbf{ij}}(\hat{s}^+_{\mathbf{i}A}\hat{s}^-_{\mathbf{j}B} + \hat{s}^-_{\mathbf{i}A}\hat{s}^+_{\mathbf{j}B} + 2\eta\hat{s}^z_{\mathbf{i}A}\hat{s}^z_{\mathbf{j}B}), \quad (1)$$

where σ indexes the layers, η characterizes the relative strength between Ising and exchange couplings, and $\mathbf{i} = (i_x, i_y)$ stands for a two-dimensional coordinate in which i_x, i_y run along the positions in a given two-dimensional layer of size $N = L \times L$. As is customary, the spin operators $\hat{s}^\alpha_{\mathbf{i}} = \hat{\sigma}^\alpha_{\mathbf{i}}/2$ are given in terms of the Pauli matrices $\hat{\sigma}^{x,y,z}$ that act on the spin at site $\mathbf{i}$. We shall focus our attention on dipole couplings of the form

$$V^{\sigma\sigma'}_{\mathbf{ij}} = \frac{J}{|\mathbf{r}^\sigma_{\mathbf{i}} - \mathbf{r}^{\sigma'}_{\mathbf{j}}|^3}\left(1 - \frac{3[\mathbf{d}\cdot(\mathbf{r}^\sigma_{\mathbf{i}} - \mathbf{r}^{\sigma'}_{\mathbf{j}})]^2}{|\mathbf{r}^\sigma_{\mathbf{i}} - \mathbf{r}^{\sigma'}_{\mathbf{j}}|^2}\right), \quad (2)$$

where $\hat{\mathbf{d}} = \sin\Theta_0\hat{e}_x + \cos\Theta_0\hat{e}_z$ is the orientation of the dipoles, $\mathbf{r}^\sigma_{\mathbf{i}}$ is the position of a dipole in layer σ, and J is the spin-exchange constant.

Motivated by recent experiments on polar molecules in bilayers [15], we consider in the following the non-equilibrium dynamics of this system starting from an initial state where all dipoles in layer A (B) are initially in the spin up (down) state. We first analyse the spin excitations in terms of a Bogoliubov treatment, and then by simulating the quantum dynamics of the full dipolar spin model using the discrete truncated Wigner approximation (DTWA) [50, 51].

Bogoliubov Analysis: As in the standard spin wave analysis, the spin dynamics can be described by mapping the Hamiltonian (1) to a hard-core bosonic model using the Holstein-Primakoff transformation $\hat{s}^z_{A,\mathbf{i}} = 1/2 - \hat{a}^\dagger_{\mathbf{i}}\hat{a}_{\mathbf{i}}$, $\hat{s}^+_{A,\mathbf{i}} = \hat{a}_{\mathbf{i}}$, $\hat{s}^-_{A,\mathbf{i}} = \hat{a}^\dagger_{\mathbf{i}}$, and $\hat{s}^z_{B,\mathbf{i}} = -1/2 + \hat{b}^\dagger_{\mathbf{i}}\hat{b}_{\mathbf{i}}$, $\hat{s}^+_{B,\mathbf{i}} = \hat{b}^\dagger_{\mathbf{i}}$, $\hat{s}^-_{B,\mathbf{i}} = \hat{b}_{\mathbf{i}}$. The bosonic operators $\hat{a}_{\mathbf{i}}$ and $\hat{b}_{\mathbf{i}}$ characterize the spin excitations that appear on top of the prepared initial state. Assuming a small population of spin excitations, much smaller than the number of sites, the Hamiltonian may be rewritten in quasi-momentum space

$$\hat{H} = \sum_{\mathbf{k}} \tilde{\varepsilon}_{\mathbf{k}}(\hat{a}^\dagger_{\mathbf{k}}\hat{a}_{\mathbf{k}} + \hat{b}^\dagger_{\mathbf{k}}\hat{b}_{\mathbf{k}}) + \Omega_{\mathbf{k}}\hat{a}^\dagger_{\mathbf{k}}\hat{b}^\dagger_{-\mathbf{k}} + \Omega^*_{\mathbf{k}}\hat{b}_{-\mathbf{k}}\hat{a}_{\mathbf{k}}, \quad (3)$$

where $\hat{a}_{\mathbf{k}} = \frac{1}{\sqrt{N}}\sum_{\mathbf{r}_{\mathbf{i}}} e^{-i\mathbf{k}\cdot\mathbf{r}_{\mathbf{i}}}\hat{a}_{\mathbf{i}}$ and $\hat{b}_{\mathbf{k}} = \frac{1}{\sqrt{N}}\sum_{\mathbf{r}_{\mathbf{i}}} e^{-i\mathbf{k}\cdot\mathbf{r}_{\mathbf{i}}}\hat{b}_{\mathbf{i}}$.

The momentum-dependent inter-layer coupling is given by $\Omega_{\mathbf{k}} = \sum_{\mathbf{j}} V^{AB}_{0\mathbf{j}} e^{-i\mathbf{k}\cdot\mathbf{r}_{\mathbf{j}}}$, whereas the intra-layer band dispersion for spin excitations in each layer is $\tilde{\varepsilon}_{\mathbf{k}} = \varepsilon_{\mathbf{k}} - \eta(\varepsilon_0 - \Omega_0)$, with $\varepsilon_{\mathbf{k}} = \sum_{\mathbf{j}\neq 0} V^{AA}_{0\mathbf{j}} e^{-i\mathbf{k}\cdot\mathbf{r}_{\mathbf{j}}}$. Note that the Ising term results in a momentum-independent shift of the intra-layer band energy. The inter-layer coupling drives the creation of correlated pairs of excitations (one per layer) at an energy cost set by the intra-layer term.

The Hamiltonian can be diagonalized by means of a Bogoliubov transformation [52], which leads to the eigenenergies $\xi_{\mathbf{k}} = \sqrt{\tilde{\varepsilon}^2_{\mathbf{k}} - |\Omega_{\mathbf{k}}|^2}$. Crucially, $|\Omega_{\mathbf{k}_c}| > |\tilde{\varepsilon}_{\mathbf{k}_c}|$ for certain quasi-momenta $\mathbf{k}_c$, resulting in imaginary eigenenergies $\xi_{\mathbf{k}_c}$, i.e. a dynamical instability of the vacuum of spin excitations leading to the creation of correlated pairs. The instability manifests itself as an exponential growth in the population of the corresponding mode, $N_{\mathbf{k}_c} = (|\Omega_{k_c}|/|\xi_{\mathbf{k}_c}|)^2 \sinh^2(|\xi_{\mathbf{k}_c}|t)$. These predictions are shown as the dashed lines in Fig. 1(b), compared to the full spin dynamics discussed below.

Note that if $a_Z^3 \gg a^3$, the inter-layer coupling $|\Omega_{\mathbf{k}}|$ is much smaller than the intra-layer bandwidth. As a result, imaginary eigen-energies only occur for $\tilde{\varepsilon}_{\mathbf{k}} \simeq 0$. This condition is modified by the shift induced by the Ising term, which hence acts as an additional knob to tailor the quasi-momentum distributions discussed below (a similar control knob would be provided by a layer bias of the form $\sum_i(\hat{s}^z_{A,\mathbf{i}} - \hat{s}^z_{B,\mathbf{i}})$). In the following, however, we focus for simplicity in the case $\eta = 0$, i.e. in the absence of Ising term (XY model), for which $\tilde{\varepsilon}_{\mathbf{k}} = \varepsilon_{\mathbf{k}}$. For the case of electric dipoles, this is achieved at zero electric field. Figure 2(a) shows the pair coupling strength $\Omega_{\mathbf{k}}$ in the Brillouin zone, overlaid with the resonant line for which $\varepsilon_{\mathbf{k}} \simeq 0$. Pairs are most effectively produced exactly on resonance and for momenta where pair coupling is strong. This is borne out in Fig. 2(b), which shows

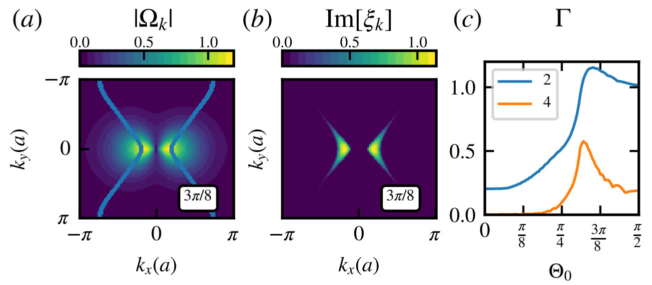

FIG. 2. Bogoliubov Analysis. (a) Pair coupling strength $|\Omega_k|$ as a colorplot, overlaid with the resonant surface $\varepsilon(k) \simeq 0$. (b) Imaginary part of the Bogoliubov energy ξ_k. Both for a dipole orientation $\Theta_0 = 3\pi/8$ and $a_Z/a = 2$. (c) Growth rate of the maximally unstable mode $\Gamma = \max_k \text{Im}[\xi_k]$ as a function of the dipole orientation Θ_0 at $a_Z/a = 2, 4$ as indicated in legend. All in units of $J/\hbar$.

the growth rate of momentum modes, i.e. the imaginary part of the Bogoliubov energy, which matches with the overlap of the resonant surface and the region of strong inter-layer coupling seen in Fig. 2(a). Bogoliubov theory hence predicts the creation of pairs with a specific quasi-momentum distribution.

Figure 2(c) shows the growth rate Γ of the most unstable mode, i.e. the maximum of the imaginary part of the Bogoliubov energies, as a function of the dipole orientation Θ_0 for two different bilayer spacings a_Z. At sufficiently long times, the most unstable modes eventually dominate pair creation, resulting in vastly different dynamical scales for the spin excitations for different dipole orientations. Note that the growth rate is the lowest at small Θ_0 and maximal close to $3\pi/8$. Since the overall form of the growth rate does not qualitatively change for $a_Z^3 \gg a^3$, we focus on the case $a_Z/a = 2$.

As shown in the quasi-momentum distributions, the most unstable mode is not unique but rather degenerate for a set of quasi-momentum modes, η_c, and hence the system evolves into the state $|\psi(t)\rangle \simeq e^{\Gamma t \sum_{\mathbf{k}\in\eta_c} \beta^\dagger_{\mathbf{k}}\beta_{\mathbf{k}}}|\text{vac}\rangle$, where $|\text{vac}\rangle$ is the vacuum of excitations, and $\beta_{\mathbf{k}}$ are the quasiparticle operators. Any linear combination of the most unstable modes is equally unstable, and hence exponential growth magnifies quantum fluctuations resulting in the population of a shot-to-shot dependent linear superposition of the modes. Thus, the population of a given mode $\mathbf{k} \in \eta_c$ presents a super-Poissonian variance (not shown). Moreover, excitations pairs are always created with opposite momenta, and hence for a given shot, the momentum distribution at momentum $\mathbf{k}$ in the layer A equals that at momentum $-\mathbf{k}$ in layer B. This behavior reflects the strongly entangled character of the state generated during pair creation.

Full spin dynamics: We next turn to the full quantum spin dynamics of the model obtained within the DTWA [50, 51]. The momentum state population of excitations in layer B maps to the structure factor which in terms of spin-operators can be written as

$$\hat{N}^B_{\mathbf{k}} = \frac{1}{N}\sum_{\mathbf{ij}} e^{i\mathbf{k}\cdot(\mathbf{r_i}-\mathbf{r_j})}\hat{b}^\dagger_{\mathbf{i}}\hat{b}_{\mathbf{j}} = \frac{1}{N}\sum_{\mathbf{ij}} e^{i\mathbf{k}\cdot(\mathbf{r_i}-\mathbf{r_j})}\hat{s}^+_{\mathbf{i}}\hat{s}^-_{\mathbf{j}} \quad (4)$$

and a similar expression holds for layer A. We define $N_{\mathbf{k}} = \langle \hat{N}^A_{\mathbf{k}}\rangle = \langle \hat{N}^B_{\mathbf{k}}\rangle$. This establishes a connection between the Bogoliubov predictions and the Fourier-transform of the spin-spin correlations, which we can obtain from the DTWA simulations of the spin dynamics. We will focus exclusively on the momentum structure here due to this correspondence (see [52] for the real-space results).

Figure 1(b) shows the population $N_{k^*}(t)$ of the most unstable mode k^* for different dipole orientations Θ_0 obtained from both DTWA simulations (solid lines) and the Bogoliubov analysis (dashed lines) with no fitting parameters. Both results are in very good agreement in the initial exponential growth regime (regime I), in which a significant number of pairs are created before corrections or further scattering terms become important. This is followed in the full dynamics by a slow down and eventual saturation to a maximal mode occupation (regime II), after which scattering between momentum modes starts to deplete the maximally unstable mode (III). As expected from the Bogoliubov analysis, we observe that the spatial and temporal growth of correlations exhibit a strong dependence on the dipole orientation.

We next turn to the time evolution of the full momentum distribution of the created pairs during the spin dynamics of the model, obtained within DTWA for a representative $\Theta_0 = 3\pi/8$ in Fig. 3(a), with an extended set of figures provided in the SI [52]. At very short times off-resonant non exponentially growing modes dominate the structure (left panel), which then give way to the exponentially growing unstable modes resulting in the distribution expected from the Bogoliubov prediction (second panel). As the most unstable modes reach saturation, growth can still occur in these unstable modes but at a lower growth rates. Naturally, higher-order terms neglected within the Bogoliubov approximation will eventually result in scattering between different momentum modes leading to prethermal behaviors followed up by thermalisation. We see this expectation borne out in the last two panels showing first an increase of population in the slower growing unstable modes and then the momentum distribution becoming uniform in the late time regime of the dynamics. We note that this subsequent approach to equilibrium can itself host rich physics [53–56]

Having observed the emergence of the predicted momentum instability in an appropriate time window for a single dipole orientation, we next compare in Fig. 3(b) the DTWA results to the Bogoliubov predictions for different dipole orientations Θ_0. Here, we choose an

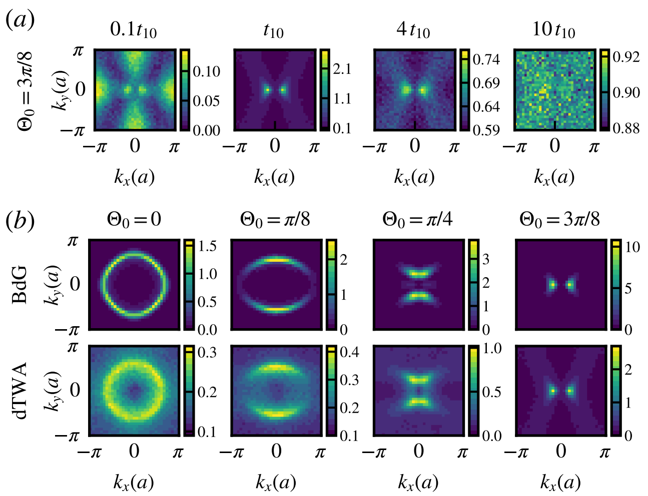

FIG. 3. Momentum structure of created pairs $N_{\mathbf{k}}$. (a) Time evolution of $N_{\mathbf{k}}(t)$ within DTWA showing the different regimes of dynamics for $\Theta_0 = 3\pi/8$. Time in terms of t_{10}, where $N_{\mathrm{pair}}(t_{10}) = 0.1N$. The left most panel shows the early time regime before exponential growth has taken over. The second panel shows the build up of the expected momentum structure. The last two panels show the subsequent thermalisation as scattering between momentum modes occurs. (b) Comparison of Bogoliubov prediction (top) and spin dynamics from DTWA (bottom) for a range of Θ_0, all at t_{10}. Results for a 33×33 bilayer with layer spacing $a_Z/a = 2$ with open boundary conditions at unit filling.

evolution time t such that the total number of pairs $N_{\mathrm{pair}} = \sum_{\mathbf{k}} N_{\mathbf{k}}(t) = 0.1N$, to allow time for the dynamical instability to create pairs, while at the same time keeping within the regime of validity of the Bogoliubov analysis. In addition, this allows us to compare different dipole orientations, which we have shown above to have vastly different dynamical growth rates. We observe good agreement for all dipole orientations indicating that the pair production mechanism is still effective in the full dipolar spin model. The good quantitative agreement between the Bogoliubov and the DTWA numerical results shows that there is indeed a time regime for all considered dipole orientations in which the momentum selective pair instability generates a large number of excitations with a characteristic momentum distribution without disruption from competing scattering processes.

This demonstrates the existence of highly-tunable set of momentum-dependent instabilities in the full dipolar spin dynamics. Changing the dipole orientation does not only lead to different time scales for the spin dynamics, but also allows for the tuning between different topologies of the unstable surface in momentum space: from a simply-connected circular manifold at $\Theta_0 = 0$, to two disconnected arcs above a critical Θ_0.

Imperfect filling: Considering the feasibility to observe these effects in an experimental setting, while tweezer arrays offer the possibility to achieve unit filling [20–23, 57–59], a major challenge in optical lattices, especially for polar molecules, is imposed by imperfect filling, which results in positional disorder of the pinned dipoles. While important developments in cooling and trapping molecules have allowed the preparation of lattice arrays with up to $f = 0.25$ [18, 60–62], which highlight the near-future potential of achieving high filling fractions, they also illustrate the need to understand which effects would be observable at lower filling fractions in current setups.

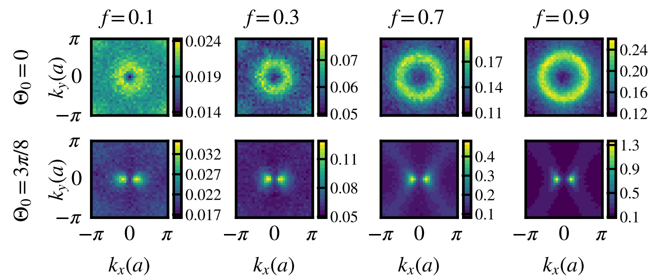

FIG. 4. Momentum occupation $N_{\mathbf{k}}$ of created pairs in presence of positional disorder/non-unit filling obtained within DTWA. Results for a range of Θ_0 and filling fraction f at fixed $a_Z/a = 2$ at times such that $N_{\mathrm{pair}}(t) = 0.1fN$. $L = 33$ with open boundary conditions.

To address this question, we consider bilayers in which each lattice site has a fixed spatially uniform probability f to be occupied or empty. We show the resulting momentum occupation N_k for different filling fractions f (averaging over 10000 filling realizations) and two dipole orientations Θ_0 in Fig. 4. Also for the case of imperfect filling our DTWA results are in very good agreement with the Bogoliubov analysis (for more details see [52]). We observe that while the signal to noise deteriorates as the lattice becomes more sparsely filled, most importantly, the main qualitative phenomenology, the emergence of a manifold of unstable exponentially growing modes, does extend to a remarkably low filling fraction regime, which makes the observation in experimental platforms feasible.

Outlook: Dipolar systems confined in two-dimensional bilayers host a rich non-equilibrium dynamics characterized by the momentum-selective creation of pairs of spin excitations. Making use of the wide tunability of dipolar interactions, one can access different shapes and topologies of the momentum distribution of the created pairs. These distributions may be probed using spatially-resolved measurements accessible in state-of-the-art platforms in tweezers and quantum gas microscopes for a range of atomic or molecular gases.

Our work opens various intriguing avenues. Although pair creation is largely robust to positional disorder in partially filled lattices, disorder may have more relevant effects on the subsequent spin dynamics on the two-dimensional bilayers, including unconventional localisation and transport properties [63, 64], and a synchronisation transition [65]. Moreover, magnetic atoms, Rydberg atoms and polar molecules offer access to multiple levels beyond the spin-1/2 system considered here, opening further opportunities to introduce chirality in the interactions, and potentially generate topological excitations [66]. Finally, the long-time behaviour and eventual thermalisation of the excitations, as well as the dependence on filling fraction and dipolar orientation, remain an open question. Since the initial pairing instability creates a well-defined highly non-thermal occupation in momentum space, the eventual approach to equilibrium might reveal universal non-equilibrium scaling exponents and self-similiarity, potentially even richer than previously studied cases [53–56], due to the correlated nature of the created state.

Acknowledgements: We acknowledge careful review of this manuscript and useful comments from A. Carroll and J. Higgins. G.A.D.-C. and L.S. acknowledge support of the Deutsche Forschungsgemeinschaft (DFG, German Research Foundation) under Germany's Excellence Strategy – EXC-2123 QuantumFrontiers – 390837967. D.W and A.M.R. acknowledge support from the AFOSR MURI, the ARO single investigator award W911NF-19-1-0210, the NSF JILA-PFC PHY-1734006 grants, NSF QLCI-2016244 grants, by the DOE Quantum Systems Accelerator (QSA) grant and by NIST.

[1] M. A. Baranov, M. Dalmonte, G. Pupillo, and P. Zoller, Condensed matter theory of dipolar quantum gases, Chemical Reviews **112**, 5012 (2012).
[2] J. L. Bohn, A. M. Rey, and J. Ye, Cold molecules: Progress in quantum engineering of chemistry and quantum matter, Science **357**, 1002 (2017).
[3] S. A. Moses, J. P. Covey, M. T. Miecnikowski, D. S. Jin, and J. Ye, New frontiers for quantum gases of polar molecules, Nat. Phys. **13**, 13 (2017).
[4] L. Chomaz, I. Ferrier-Barbut, F. Ferlaino, B. Laburthe-Tolra, B. L. Lev, and T. Pfau, Dipolar physics: a review of experiments with magnetic quantum gases, Reports on Progress in Physics **86**, 026401 (2023).
[5] A. Browaeys and T. Lahaye, Many-body physics with individually controlled Rydberg atoms, Nat. Phys. **16**, 132 (2020).
[6] M. Saffman, T. G. Walker, and K. Mølmer, Quantum information with rydberg atoms, Rev. Mod. Phys. **82**, 2313 (2010).
[7] S. de Léséleuc, V. Lienhard, P. Scholl, D. Barredo, S. Weber, N. Lang, H. P. Büchler, T. Lahaye, and A. Browaeys, Observation of a symmetry-protected topological phase of interacting bosons with rydberg atoms, Science **365**, 775 (2019).
[8] B. Yan, S. A. Moses, B. Gadway, J. P. Covey, K. R. A. Hazzard, A. M. Rey, D. S. Jin, and J. Ye, Observation of dipolar spin-exchange interactions with lattice-confined polar molecules, Nature **501**, 521 (2013).
[9] A. de Paz, A. Sharma, A. Chotia, E. Maréchal, J. H. Huckans, P. Pedri, L. Santos, O. Gorceix, L. Vernac, and B. Laburthe-Tolra, Nonequilibrium quantum magnetism in a dipolar lattice gas, Phys. Rev. Lett. **111**, 185305 (2013).
[10] K. R. A. Hazzard, B. Gadway, M. Foss-Feig, B. Yan, S. A. Moses, J. P. Covey, N. Y. Yao, M. D. Lukin, J. Ye, D. S. Jin, and A. M. Rey, Many-body dynamics of dipolar molecules in an optical lattice, Phys. Rev. Lett. **113**, 195302 (2014).
[11] S. Lepoutre, J. Schachenmayer, L. Gabardos, B. Zhu, B. Naylor, E. Maréchal, O. Gorceix, A. M. Rey, L. Vernac, and B. Laburthe-Tolra, Out-of-equilibrium quantum magnetism and thermalization in a spin-3 many-body dipolar lattice system, Nature Communications **10**, 1714 (2019).
[12] L. Gabardos, B. Zhu, S. Lepoutre, A. M. Rey, B. Laburthe-Tolra, and L. Vernac, Relaxation of the collective magnetization of a dense 3d array of interacting dipolar $s = 3$ atoms, Phys. Rev. Lett. **125**, 143401 (2020).
[13] A. Patscheider, B. Zhu, L. Chomaz, D. Petter, S. Baier, A.-M. Rey, F. Ferlaino, and M. J. Mark, Controlling dipolar exchange interactions in a dense three-dimensional array of large-spin fermions, Phys. Rev. Res. **2**, 023050 (2020).
[14] T. Bilitewski, L. De Marco, J.-R. Li, K. Matsuda, W. G. Tobias, G. Valtolina, J. Ye, and A. M. Rey, Dynamical generation of spin squeezing in ultracold dipolar molecules, Phys. Rev. Lett. **126**, 113401 (2021).
[15] W. G. Tobias, K. Matsuda, J.-R. Li, C. Miller, A. N. Carroll, T. Bilitewski, A. M. Rey, and J. Ye, Reactions between layer-resolved molecules mediated by dipolar spin exchange, Science **375**, 1299 (2022).
[16] T. Bilitewski and A. M. Rey, Manipulating growth and propagation of correlations in dipolar multilayers: From pair production to bosonic Kitaev models, arXiv:2211.12521 [quant-ph] (2022).
[17] J.-R. Li, K. Matsuda, C. Miller, A. N. Carroll, W. G. Tobias, J. S. Higgins, and J. Ye, Tunable itinerant spin dynamics with polar molecules, Nature **614**, 70 (2023).
[18] L. Christakis, J. S. Rosenberg, R. Raj, S. Chi, A. Morningstar, D. A. Huse, Z. Z. Yan, and W. S. Bakr, Probing site-resolved correlations in a spin system of ultracold molecules, Nature **614**, 64 (2023).
[19] C. Gross and W. S. Bakr, Quantum gas microscopy for single atom and spin detection, Nature Physics **17**, 1316 (2021).
[20] A. M. Kaufman and K.-K. Ni, Quantum science with optical tweezer arrays of ultracold atoms and molecules, Nature Physics **17**, 1324 (2021).
[21] C. M. Holland, Y. Lu, and L. W. Cheuk, On-Demand Entanglement of Molecules in a Reconfigurable Optical Tweezer Array, arXiv:2210.06309 [cond-mat.quant-gas] (2022).
[22] Y. Bao, S. S. Yu, L. Anderegg, E. Chae, W. Ketterle, K.-K. Ni, and J. M. Doyle, Dipolar spin-exchange and entanglement between molecules in an optical tweezer array, arXiv:2211.09780 [physics.atom-ph] (2022).
[23] L. Anderegg, L. W. Cheuk, Y. Bao, S. Burchesky, W. Ketterle, K.-K. Ni, and J. M. Doyle, An optical tweezer array of ultracold molecules, Science **365**, 1156 (2019).
[24] J. T. Zhang, Y. Yu, W. B. Cairncross, K. Wang, L. R. B. Picard, J. D. Hood, Y.-W. Lin, J. M. Hutson, and K.-K.

Ni, Forming a Single Molecule by Magnetoassociation in an Optical Tweezer, Phys. Rev. Lett. **124**, 253401 (2020).
[25] A. Einstein, B. Podolsky, and N. Rosen, Can quantum-mechanical description of physical reality be considered complete?, Phys. Rev. **47**, 777 (1935).
[26] M. D. Reid, P. D. Drummond, W. P. Bowen, E. G. Cavalcanti, P. K. Lam, H. A. Bachor, U. L. Andersen, and G. Leuchs, Colloquium: The einstein-podolsky-rosen paradox: From concepts to applications, Rev. Mod. Phys. **81**, 1727 (2009).
[27] M. Fadel, T. Zibold, B. Décamps, and P. Treutlein, Spatial entanglement patterns and einstein-podolsky-rosen steering in bose-einstein condensates, Science **360**, 409 (2018).
[28] P. Kunkel, M. Prüfer, H. Strobel, D. Linnemann, A. Frölian, T. Gasenzer, M. Gärttner, and M. K. Oberthaler, Spatially distributed multipartite entanglement enables epr steering of atomic clouds, Science **360**, 413 (2018).
[29] G. Agarwal, *Quantum Optics*, Quantum Optics (Cambridge University Press, 2013).
[30] J. Schwinger, On gauge invariance and vacuum polarization, Phys. Rev. **82**, 664 (1951).
[31] P. Hauke, D. Marcos, M. Dalmonte, and P. Zoller, Quantum simulation of a lattice schwinger model in a chain of trapped ions, Phys. Rev. X **3**, 041018 (2013).
[32] V. Kasper, F. Hebenstreit, M. Oberthaler, and J. Berges, Schwinger pair production with ultracold atoms, Physics Letters B **760**, 742 (2016).
[33] W. G. Unruh, Notes on black-hole evaporation, Phys. Rev. D **14**, 870 (1976).
[34] J. Hu, L. Feng, Z. Zhang, and C. Chin, Quantum simulation of unruh radiation, Nature Physics **15**, 785 (2019).
[35] Y. Takahashi and H. Umezawa, Thermo field dynamics, International Journal of Modern Physics B **10**, 1755 (1996).
[36] S. Chapman, J. Eisert, L. Hackl, M. P. Heller, R. Jefferson, H. Marrochio, and R. C. Myers, Complexity and entanglement for thermofield double states, SciPost Physics **6** (2019).
[37] D. Zhu, S. Johri, N. M. Linke, K. A. Landsman, C. H. Alderete, N. H. Nguyen, A. Y. Matsuura, T. H. Hsieh, and C. Monroe, Generation of thermofield double states and critical ground states with a quantum computer, Proceedings of the National Academy of Sciences **117**, 25402 (2020).
[38] P. Gao, D. L. Jafferis, and A. C. Wall, Traversable wormholes via a double trace deformation, Journal of High Energy Physics **2017** (2017).
[39] J. Maldacena, D. Stanford, and Z. Yang, Diving into traversable wormholes, Fortschritte der Physik **65**, 1700034 (2017).
[40] C. Gross, H. Strobel, E. Nicklas, T. Zibold, N. Bar-Gill, G. Kurizki, and M. K. Oberthaler, Atomic homodyne detection of continuous-variable entangled twin-atom states, Nature **480**, 219 (2011).
[41] B. Lücke, M. Scherer, J. Kruse, L. Pezzé, F. Deuretzbacher, P. Hyllus, O. Topic, J. Peise, W. Ertmer, J. Arlt, L. Santos, A. Smerzi, and C. Klempt, Twin matter waves for interferometry beyond the classical limit, Science **334**, 773 (2011).
[42] A. Sørensen, L.-M. Duan, J. I. Cirac, and P. Zoller, Many-particle entanglement with bose–einstein condensates, Nature **409**, 63 (2001).
[43] A. Qu, B. Evrard, J. Dalibard, and F. Gerbier, Probing spin correlations in a bose-einstein condensate near the single-atom level, Phys. Rev. Lett. **125**, 033401 (2020).
[44] C. Klempt, O. Topic, G. Gebreyesus, M. Scherer, T. Henninger, P. Hyllus, W. Ertmer, L. Santos, and J. J. Arlt, Multiresonant spinor dynamics in a bose-einstein condensate, Phys. Rev. Lett. **103**, 195302 (2009).
[45] B. Sundar, D. Barberena, A. P. Orioli, A. Chu, J. K. Thompson, A. M. Rey, and R. J. Lewis-Swan, Bosonic pair production and squeezing for optical phase measurements in long-lived dipoles coupled to a cavity, arXiv:2204.13090 [quant-ph] (2022).
[46] A. Periwal, E. S. Cooper, P. Kunkel, J. F. Wienand, E. J. Davis, and M. Schleier-Smith, Programmable interactions and emergent geometry in an array of atom clouds, Nature **600**, 630 (2021).
[47] J. Nipper, J. B. Balewski, A. T. Krupp, S. Hofferberth, R. Löw, and T. Pfau, Atomic pair-state interferometer: Controlling and measuring an interaction-induced phase shift in rydberg-atom pairs, Phys. Rev. X **2**, 031011 (2012).
[48] M. L. Wall, K. R. A. Hazzard, and A. M. Rey, Quantum magnetism with ultracold molecules, in *From Atomic to Mesoscale* (WORLD SCIENTIFIC, 2015) pp. 3–37.
[49] C. Chen, G. Bornet, M. Bintz, G. Emperauger, L. Leclerc, V. S. Liu, P. Scholl, D. Barredo, J. Hauschild, S. Chatterjee, M. Schuler, A. M. Laeuchli, M. P. Zaletel, T. Lahaye, N. Y. Yao, and A. Browaeys, Continuous Symmetry Breaking in a Two-dimensional Rydberg Array, arXiv:2207.12930 [cond-mat.quant-gas] (2022).
[50] J. Schachenmayer, A. Pikovski, and A. M. Rey, Many-body quantum spin dynamics with monte carlo trajectories on a discrete phase space, Phys. Rev. X **5**, 011022 (2015).
[51] B. Zhu, A. M. Rey, and J. Schachenmayer, A generalized phase space approach for solving quantum spin dynamics, New Journal of Physics **21**, 082001 (2019).
[52] See Supplemental Material at [URL will be inserted by publisher] for additional details on the Bogoliubov analysis, the effect of boundary conditions, the real space structure of the spin correlations, and Bogoliubov as well as extended dTWA results for the finite filling fraction behavior, and extended dTWA results for the time-dependence of the momentum structure of correlations.
[53] M. Prüfer, P. Kunkel, H. Strobel, S. Lannig, D. Linnemann, C.-M. Schmied, J. Berges, T. Gasenzer, and M. K. Oberthaler, Observation of universal dynamics in a spinor bose gas far from equilibrium, Nature **563**, 217 (2018).
[54] S. Erne, R. Bücker, T. Gasenzer, J. Berges, and J. Schmiedmayer, Universal dynamics in an isolated one-dimensional bose gas far from equilibrium, Nature **563**, 225 (2018).
[55] J. A. P. Glidden, C. Eigen, L. H. Dogra, T. A. Hilker, R. P. Smith, and Z. Hadzibabic, Bidirectional dynamic scaling in an isolated bose gas far from equilibrium, Nature Physics **17**, 457 (2021).
[56] J. F. Rodriguez-Nieva, A. P. Orioli, and J. Marino, Far-from-equilibrium universality in the two-dimensional heisenberg model, Proceedings of the National Academy of Sciences **119** (2022).
[57] M. Endres, H. Bernien, A. Keesling, H. Levine, E. R. Anschuetz, A. Krajenbrink, C. Senko, V. Vuletic, M. Greiner, and M. D. Lukin, Atom-by-atom assembly

of defect-free one-dimensional cold atom arrays, Science **354**, 1024 (2016).

[58] D. Barredo, S. de Léséleuc, V. Lienhard, T. Lahaye, and A. Browaeys, An atom-by-atom assembler of defect-free arbitrary two-dimensional atomic arrays, Science **354**, 1021 (2016).

[59] J. T. Zhang, L. R. B. Picard, W. B. Cairncross, K. Wang, Y. Yu, F. Fang, and K.-K. Ni, An optical tweezer array of ground-state polar molecules, Quantum Science and Technology **7**, 035006 (2022).

[60] L. De Marco, G. Valtolina, K. Matsuda, W. G. Tobias, J. P. Covey, and J. Ye, A degenerate Fermi gas of polar molecules, Science **363**, 853 (2019).

[61] G. Valtolina, K. Matsuda, W. G. Tobias, J.-R. Li, L. D. Marco, and J. Ye, Dipolar evaporation of reactive molecules to below the fermi temperature, Nature **588**, 239 (2020).

[62] S. A. Moses, J. P. Covey, M. T. Miecnikowski, B. Yan, B. Gadway, J. Ye, and D. S. Jin, Creation of a low-entropy quantum gas of polar molecules in an optical lattice, Science **350**, 659 (2015).

[63] T. Xu and R. V. Krems, Quantum walk and anderson localization of rotational excitations in disordered ensembles of polar molecules, New Journal of Physics **17**, 065014 (2015).

[64] X. Deng, B. L. Altshuler, G. V. Shlyapnikov, and L. Santos, Quantum levy flights and multifractality of dipolar excitations in a random system, Phys. Rev. Lett. **117**, 020401 (2016).

[65] M. P. Kwasigroch and N. R. Cooper, Synchronization transition in dipole-coupled two-level systems with positional disorder, Phys. Rev. A **96**, 053610 (2017).

[66] S. V. Syzranov, M. L. Wall, V. Gurarie, and A. M. Rey, Spin–orbital dynamics in a system of polar molecules, Nature Communications **5** (2014).

Supplementary Information

The supplementary information contains additional details on the Bogoliubov analysis, the effect of boundary conditions, the real space structure of the spin correlations, and Bogoliubov as well as extended DTWA results for the finite filling fraction behavior of the momentum structure of correlations, and extended DTWA results for the time-dependence.

Bogoliubov Analysis

In this section, we provide further details on the Bogoliubov analysis of the spin Hamiltonian. First, we focus on the diagonalization procedure of a unit filling lattice, then we proceed to discuss the case of lattices with fillings smaller than one. For a perfectly filled lattice, we may write the Hamiltonian in quasi-momentum space:

$$\begin{aligned}\hat{H} = &\sum_{\mathbf{k}} \varepsilon_{\mathbf{k}} (\hat{a}^{\dagger}_{\mathbf{k}} \hat{a}_{\mathbf{k}} + \hat{b}^{\dagger}_{\mathbf{k}} \hat{b}_{\mathbf{k}}) + \\ &\sum_{\mathbf{k}} | \left[\Omega_{\mathbf{k}} | e^{-i\alpha_{\mathbf{k}}} \hat{a}^{\dagger}_{\mathbf{k}} \hat{b}^{\dagger}_{-\mathbf{k}} + |\Omega_{\mathbf{k}}| e^{i\alpha_{\mathbf{k}}} \hat{a}_{\mathbf{k}} \hat{b}_{-\mathbf{k}} \right],\end{aligned} \tag{S1}$$

where we have made explicit the complex nature of the inter-layer coupling $\Omega_{\mathbf{k}} = |\Omega_{\mathbf{k}}| e^{-i\alpha_{\mathbf{k}}}$. In the presence of an Ising term, we would simply substitute $\varepsilon_{\mathbf{k}}$ by $\tilde{\varepsilon}_{\mathbf{k}}$. Before introducing the Bogoliubov transformation it is convenient to decouple the above Hamiltonian into symmetric and antisymmetric collective quasi-momentum modes. For this purpose, we define the following operators

$$\begin{aligned}\hat{S}_{\mathbf{k}} &= \frac{1}{\sqrt{2}} (e^{-i\alpha_{\mathbf{k}}/2} \hat{a}_{\mathbf{k}} + e^{i\alpha_{\mathbf{k}}/2} \hat{b}_{\mathbf{k}}) \\ \hat{A}_{\mathbf{k}} &= \frac{1}{\sqrt{2}} (e^{-i\alpha_{\mathbf{k}/2}} \hat{a}_{\mathbf{k}} - e^{i\alpha_{\mathbf{k}}} \hat{b}_{\mathbf{k}}).\end{aligned} \tag{S2}$$

In terms of these new operators, the Hamiltonian can be rewritten as $\hat{H} = \hat{H}_S + \hat{H}_A$ with

$$\begin{aligned}\hat{H}_S &= \sum_{\mathbf{k}} \varepsilon_{\mathbf{k}} \hat{S}^{\dagger}_{\mathbf{k}} \hat{S}_{\mathbf{k}} + \frac{|\Omega_{\mathbf{k}}|}{2} (\hat{S}^{\dagger}_{\mathbf{k}} \hat{S}^{\dagger}_{-\mathbf{k}} + \hat{S}_{\mathbf{k}} \hat{S}_{-\mathbf{k}}) \\ \hat{H}_A &= \sum_{\mathbf{k}} \varepsilon_{\mathbf{k}} \hat{A}^{\dagger}_{\mathbf{k}} \hat{A}_{\mathbf{k}} - \frac{|\Omega_{\mathbf{k}}|}{2} (\hat{A}^{\dagger}_{\mathbf{k}} \hat{A}^{\dagger}_{-\mathbf{k}} + \hat{A}_{\mathbf{k}} \hat{A}_{-\mathbf{k}}).\end{aligned} \tag{S3}$$

In the following, we discuss the diagonalization of $\hat{H}_S$, but that of $\hat{H}_A$ is completely analogous. At this point, we introduce the Bogoliubov transformation $\hat{\beta}_{\mathbf{k}} = u_{\mathbf{k}} \hat{S}_{\mathbf{k}} - v^{*}_{\mathbf{k}} \hat{S}^{\dagger}_{-\mathbf{k}}$. The amplitudes $u_{\mathbf{k}}$ and $v_{\mathbf{k}}$ obey the Bogoliubov-de Gennes equations:

$$\xi_{\mathbf{k}} u_{\mathbf{k}} = \varepsilon_{\mathbf{k}} u_{\mathbf{k}} + |\Omega_{\mathbf{k}}| v_{\mathbf{k}}, \tag{S4}$$

$$\xi_{\mathbf{k}} v_{\mathbf{k}} = -|\Omega_{\mathbf{k}}| u_{\mathbf{k}} - \varepsilon_{\mathbf{k}} v_{\mathbf{k}}, \tag{S5}$$

where the eigenenergies acquire the form $\xi_{\mathbf{k}} = \sqrt{\varepsilon^2_{\mathbf{k}} - |\Omega_{\mathbf{k}}|^2}$. In the case of real eigenvalues, the time dependence of the Bogoliubov operators is $\hat{\beta}_{\mathbf{k}}(t) = e^{-i\xi_{\mathbf{k}} t} \hat{\beta}_{\mathbf{k}}(0)$ and $\hat{\beta}^{\dagger}_{\mathbf{k}}(t) = e^{i\xi_{\mathbf{k}} t} \hat{\beta}^{\dagger}_{\mathbf{k}}(0)$. Inversion of the Bogoliubov transformation yields the following expression

$$\begin{aligned}\hat{S}_{\mathbf{k}}(t) = &[e^{-i\xi_{\mathbf{k}} t} \cosh^2 \phi_{\mathbf{k}} - e^{i\xi_{\mathbf{k}} t} \sinh^2 \phi_{\mathbf{k}}] \hat{S}_{\mathbf{k}}(0) + \\ &i \sinh(2\phi_{\mathbf{k}}) \sin(\xi_{\mathbf{k}} t) \hat{S}^{\dagger}_{\mathbf{k}}(0),\end{aligned} \tag{S6}$$

with $\sinh^2 2\phi_{\mathbf{k}} = |\Omega_{\mathbf{k}}|^2/\xi^2_{\mathbf{k}}$. The vacuum expectation value of the population of the symmetric mode $\mathbf{k}$ gives $\langle 0|\hat{S}^{\dagger}_{\mathbf{k}}(t) \hat{S}_{\mathbf{k}}(t)|0\rangle = \sinh^2(2\phi_{\mathbf{k}}) \sin^2(\xi_{\mathbf{k}} t)$, the same expression fulfills $\langle 0|\hat{A}^{\dagger}_{\mathbf{k}}(t) \hat{A}_{\mathbf{k}}(t)|0\rangle$. Then, the total population of the mode is simple

$$\begin{aligned}N_{\mathbf{k}} &= \langle \hat{A}^{\dagger}_{\mathbf{k}}(t) \hat{A}_{\mathbf{k}}(t) + \hat{S}^{\dagger}_{\mathbf{k}}(t) \hat{S}_{\mathbf{k}}(t) \rangle/2 \\ &= [|\Omega_{\mathbf{k}}| \sin(\xi_{\mathbf{k}} t)/\xi_{\mathbf{k}}]^2\end{aligned} \tag{S7}$$

If $\xi_{\mathbf{k}}$ is imaginary, the Bogoliubov modes fulfill $|u_{\mathbf{k}}|^2 = |v_{\mathbf{k}}|^2$ and therefore the modes are actually quadratures of the form

$$\begin{aligned}\hat{X}_{\mathbf{k}} &= \frac{1}{\sqrt{\sin \phi_{\mathbf{k}}}} \left[e^{-i\phi_{\mathbf{k}}/2} \hat{S}_{\mathbf{k}} - e^{i\phi_{\mathbf{k}}/2} \hat{S}^{\dagger}_{-\mathbf{k}} \right] \\ \hat{P}_{\mathbf{k}} &= \frac{1}{\sqrt{\sin \phi_{\mathbf{k}}}} \left[e^{i\phi_{\mathbf{k}}/2} \hat{S}_{\mathbf{k}} - e^{-i\phi_{\mathbf{k}}/2} \hat{S}^{\dagger}_{-\mathbf{k}} \right],\end{aligned} \tag{S8}$$

with $\tan \phi_{\mathbf{k}} = -\varepsilon_{\mathbf{k}}/|\xi_{\mathbf{k}}|$. The first quadrature grows exponentially in time $\hat{X}_{\mathbf{k}}(t) = e^{|\xi_{\mathbf{k}}|t} \hat{X}_{\mathbf{k}}(0)$, whereas $\hat{P}_{\mathbf{k}}(t) = e^{-|\xi_{\mathbf{k}}|t} \hat{P}_{\mathbf{k}}(0)$ decreases exponentially. By inverting the definition of the quadratures one can find the time evolution of the symmetric mode

$$\begin{aligned}\hat{S}_{\mathbf{k}} = &\frac{i}{\sqrt{2 \sin \phi_{\mathbf{k}}}} [(e^{-i\phi_{\mathbf{k}}} e^{|\xi_{\mathbf{k}}|t} - e^{i\phi_{\mathbf{k}}} e^{-|\xi_{\mathbf{k}}|t}) \hat{S}_{\mathbf{k}}(0) \\ &- 2 \sinh(|\xi_{\mathbf{k}}|t) \hat{S}^{\dagger}_{-\mathbf{k}}(0)]\end{aligned} \tag{S9}$$

then it follows that $\langle \hat{S}^{\dagger}_{\mathbf{k}}(t) \hat{S}_{\mathbf{k}}(t) \rangle = \sinh^2(|\xi_{\mathbf{k}}|t)/\sin^2 \phi^2_{\mathbf{k}}$, a similar expression fulfills $\langle \hat{A}^{\dagger}_{\mathbf{k}}(t) \hat{A}_{\mathbf{k}}(t) \rangle$. The total population of the mode is simple $N_{\mathbf{k}} = [|\Omega_{\mathbf{k}}| \sinh(|\xi_{\mathbf{k}}|t)/|\xi_{\mathbf{k}}|]^2$. Since $\sin(i|\xi_{\mathbf{k}}|)/i|\xi_{\mathbf{k}}| \to -\sinh(|\xi_{\mathbf{k}}|)/|\xi_{\mathbf{k}}|$, one can safely use the expression in Eq. (S7) to obtain the time dependence of the density of excitations in each layer

$$n(t) a^2 = \int_{BZ} \frac{d^2 k}{(2\pi)^2} |\Omega_k|^2 \left[\frac{\sin |\xi_{\mathbf{k}}| t}{|\xi_{\mathbf{k}}|} \right], \tag{S10}$$

where the integration is over the first Brillouin zone.

The Bogoliubov treatment of the case of imperfect filling is more involved. We consider a lattice with $L \times L$ sites with open boundary conditions, and a filling $f < 1$. We create a given realization by randomly filling each layer with a given number of dipoles, up to the desired lattice filling. Due to positional disorder, it is suitable to work with the Hamiltonian in space representation

$$\begin{aligned}\hat{H} = &\sum_{\mathbf{i} \neq \mathbf{j}} V^{AA}_{\mathbf{ij}} \hat{a}^{\dagger}_{\mathbf{i}} \hat{a}_{\mathbf{j}} + \sum_{\mathbf{i} \neq \mathbf{j}} V^{BB}_{\mathbf{ij}} \hat{b}^{\dagger}_{\mathbf{i}} \hat{b}_{\mathbf{j}} \\ &+ \sum_{\mathbf{i},\mathbf{j}} V^{AB}_{\mathbf{ij}} \hat{a}^{\dagger}_{\mathbf{i}} \hat{b}^{\dagger}_{\mathbf{j}} + \sum_{\mathbf{i},\mathbf{j}} V^{BA}_{\mathbf{ij}} \hat{b}_{\mathbf{i}} \hat{a}_{\mathbf{j}}.\end{aligned} \tag{S11}$$

We may again apply the Bogoliubov transformation, $\hat{\beta}_n = \sum_{\mathbf{j}} u_{n\mathbf{j}} \hat{a}_{\mathbf{j}} + \sum_{\mathbf{j}'} v_{n\mathbf{j}'} \hat{b}_{\mathbf{j}'}$. By imposing that $\xi_n \hat{\beta}_n = [\hat{\beta}_n, \hat{H}]$, we obtain the Bogoliubov-de-Gennes equations

$$\xi_n \begin{pmatrix} \mathbf{u}_n \\ \mathbf{v}_n \end{pmatrix} = \begin{pmatrix} V^{AA} & -V^{AB} \\ V^{BA} & -V^{BB} \end{pmatrix} \begin{pmatrix} \mathbf{u}_n \\ \mathbf{v}_n \end{pmatrix}, \tag{S12}$$

where $\mathbf{u}_n = (u_{n,\mathbf{i}_1}, u_{n,\mathbf{i}_2} \dots u_{n,\mathbf{i}_{L\times L}})^T$ and similarly for $\mathbf{v}_n$. By solving the above eigenvalue problem, we obtain the eigenmodes and their corresponding evolution in time. Inverting the Bogoliubov transformation provides the time dependence of the lattice operators, and Fourier transforming yields the quasi-momentum distribution. Averaging over many random realizations of the lattice filling, we obtain the distributions discussed below.

Comparison of open and closed boundary conditions

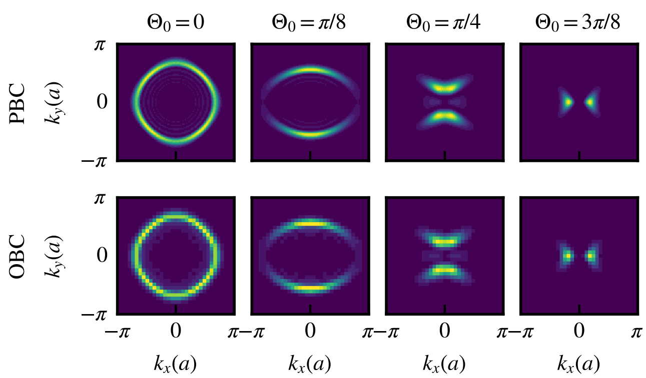

FIG. S1. Effect of the boundary conditions in the Bogoliubov analysis. We depict the quasi-momentum distribution of the created pairs, N_k, comparing periodic (top) and open (bottom) boundary conditions for a range of dipole orientations Θ_0, at times such that $N_{\text{pair}}(t) = \sum_{\mathbf{k}} N_{\mathbf{k}}(t) = 0.1N$. The results were obtained for a 33×33 bilayer with layer spacing $a_z/a = 2$ at unit filling.

The above mentioned procedure in real space for $f < 1$ may be also employed for full filling, providing the time evolution in the presence of open-boundary conditions, rather than periodic boundary conditions, as implictly assumed in the analysis in quasi-momentum space. We consider the effects of boundary conditions on the momentum structure of the created pairs in finite systems within the Bogoliubov analysis in Fig. S1. We see that both periodic (top) and open boundaries (bottom) result in basically the same momentum structure across all dipole orientations. This demonstrates that the predicted phenomena should be accessible within the limitations on total particle numbers and lattice sizes available in experimental platforms.

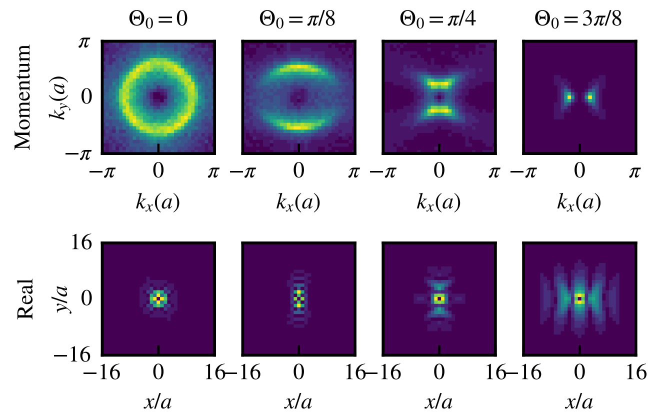

FIG. S2. Correlations in momentum and real space. Top panel spin-structure factor $S^{+-}_{\mathbf{k}}(t)$ (see S14), corresponding to momentum state population of pairs $N_k(t)$, compared to the real-space structure of spin-correlations $|C^{+-}_{\mathbf{r}}(t)|$ (see S13). Results for a 33×33 bilayer with a layer spacing of $a_Z/a = 2$ and open boundary conditions at time t such that $N_{\text{pair}}(t) = N/10$.

Comparison of momentum and real-space structure of correlations

In this section we provide results for the correlation structure in real space. While we mainly focus on the momentum structure of the correlations, as they directly map to the occupation of momentum modes and the Bogoliubov analysis, the real space correlations are what would be directly observed in an experiment with access to spatially resolved measurements.

Defining the spin-spin correlation function

$$C^{+-}_{\mathbf{ij}} = \left\langle \hat{s}^+_{\mathbf{i}} \hat{s}^-_{\mathbf{j}} \right\rangle \tag{S13}$$

the spin-structure factor $S^{A(B),+-}_{\mathbf{k}}$, which corresponds to the momentum mode occupation in the low excitation limit, is just

$$S^{A(B),+-}_{\mathbf{k}} = \frac{1}{N} \sum_{\mathbf{ij} \in A(B)} e^{i\mathbf{k}(\mathbf{r_i} - \mathbf{r_j})} C^{+-}_{\mathbf{ij}} \tag{S14}$$

We compare these expressions directly in Fig. S2 for a range of dipole orientations. The top panels shows the spin-structure factor $S^{+-}_{\mathbf{k}}$, and the bottom panels show the corresponding real-space correlation function $C^{+-}_{\mathbf{r}}$ at a distance $\mathbf{r} = \mathbf{r_i} - \mathbf{r_j}$, both summed over the layers A, B. To make the structure of real-space correlations visible on top of the population growth, we only show them for $\mathbf{i} \neq \mathbf{j}$, e.g. set $C^{+-}_{\mathbf{ii}} = 0$. These results highlight the intricate real-space structure of the correlations created during the pair-creation process. We note that up to boundary effects, the density of excitations itself is fully homogeneous throughout the dynamics, and the structure emerges within the inter-site off-diagonal correlations.

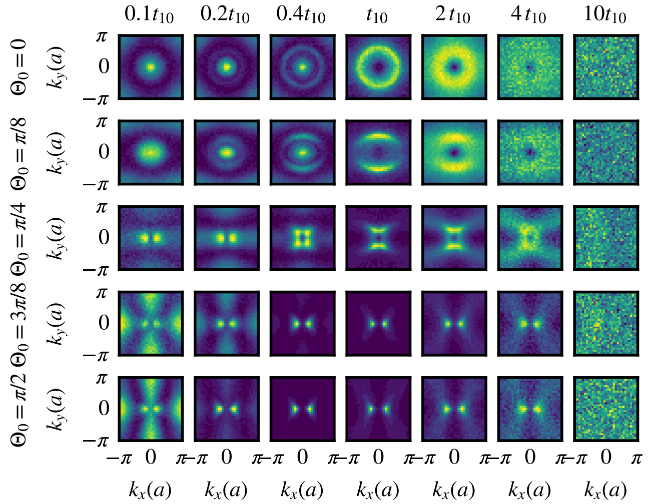

FIG. S3. Extended DTWA results on time evolution. Momentum state population of pairs $N_k(t)$ within DTWA showing the different regimes of dynamics for a range of dipole orientations Θ_0 at times in terms of t_{10} at which $N_{\rm pair}(t_{10}) = 0.1N$. The left most panel shows the early time regime before exponential growth has taken over. The second and third panel show the build up of the expected momentum structure. The central panel shows the fully built-up expected momentum structure. The last three panels show the subsequent thermalisation as scattering between momentum modes occurs. Results for a 33×33 bilayer with a layer spacing of $a_Z/a = 2$ and open boundary conditions.

Extended results on time-dependence

We provide extended results for the time-dependence of the momentum structure of the created pairs obtained within DTWA in Fig. S3. This provides both the full range of dipole orientations (in contrast to the single case of $\Theta_0 = 3\pi/8$ in the main text), as well as additional times during the build-up of correlations, as well as during the late time thermalisation state. The qualitative picture remains the same for all dipole orientations, in that at very early times, the dynamics of stable modes can dominate over the exponentially growing unstable modes, which establish the expected momentum structure at intermediate times, before scattering between modes leads to thermalisation and a homogeneous background at late times.

Results at finite filling

Figure S4 shows the quasi-momentum distribution of the created pairs for an imperfect filling within the Bogoliubov analysis, following the procedure discussed above. These results should be compared with the results shown in Fig. 4(b) of the main text, as well as with the results covering an expanded set of dipole orientations in Fig. S5. The DTWA results are averaged over 10000 realisations of the lattice occupations, whereas the Bogoliubov results average over 200 realisations.

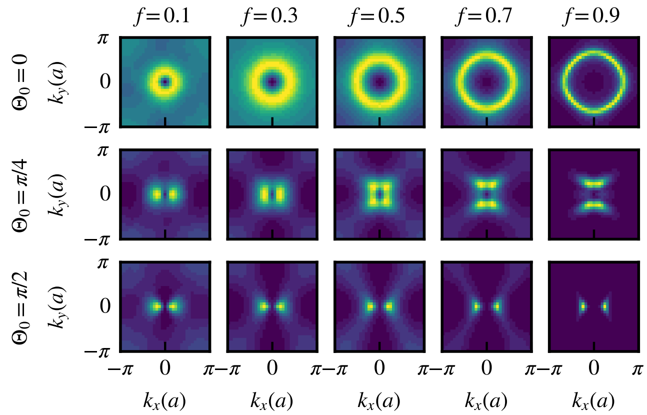

FIG. S4. Bogoliubov results at finite filling. Momentum state population N_k for a range of Θ_0 and filling fraction f at times such that $N_{\rm pair}(t) = 0.1fN$. Results for a 33×33 bilayer with a layer spacing of $a_Z/a = 2$ and open boundary conditions.

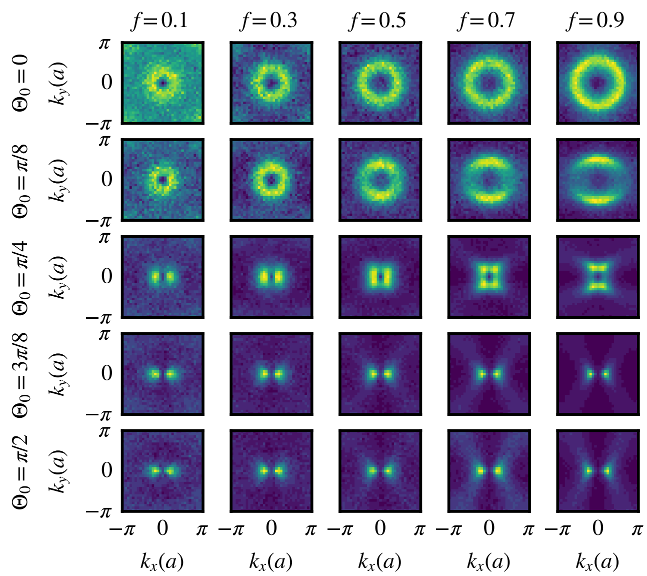

FIG. S5. Extended DTWA results at finite filling. Momentum structure of created pairs $N_{\mathbf{k}}(t)$ at times t such that the total number of pairs $N_{pair}(t) = 0.1fN$. Results for a range of Θ_0 and filling fraction f for a 33×33 bilayer with a layer spacing of $a_Z/a = 2$ and open boundary conditions

Across all dipole orientations and filling fractions we observe again a very good agreement between the spin dynamics obtained with the DTWA and the Bogoliubov predictions. In particular, both show the shrinking of the structures in momentum space as the filling fraction is lowered. Intuitively, large momentum modes would be expected to be more strongly affected by the introduction of local disorder, whereas small momentum modes would be expected to be more resilient, which seems to be the case here.

Importantly, the dynamics remains qualitatively unaffected by the imperfect filling, being still characterized by the exponential growth of characteristic patterns in quasi-momentum space, that depend on the dipole orientation. This robustness against imperfect filling is particularly relevant, since it makes feasible the observation of the effect in current experimental platforms.